Energy Nexus 10 (2023) 100200

Contents lists available at ScienceDirect

Energy Nexus

journal homepage: www.elsevier.com/locate/nexus

Full Length Article

Energy optimization of a food-energy-water microgrid living laboratory in Yukon, Canada

Daniel J. Sambor[a,*], Henry Penn[b], Mark Z. Jacobson[a]

[a] Department of Civil and Environmental Engineering, Stanford University, 473 Via Ortega, Stanford, CA 94305, United States
[b] Arctic Institute of North America, University of Calgary, 2500 University Drive NW, Calgary, AB T2N 1N4, Canada

ARTICLE INFO

Keywords:
Microgrid
Demand-side management
Solar
Food-energy-water systems

ABSTRACT

Like most northern settlements, Kluane Lake Research Station (KLRS) in Yukon Territory, Canada, is an islanded microgrid dependent on diesel generation and subject to high fuel costs. To reduce diesel costs, the station has a 48 kW solar photovoltaic (PV) array alongside a 27 kW/171 kWh lead-acid battery system to store solar energy for nighttime use, primarily during summer. However, substantial solar energy is often curtailed when the battery becomes full due to prior charging with diesel-generated electricity. The goal of this analysis is to determine how to best operate the diesel generator to maximize solar PV generation, and thus minimize diesel costs. On a monthly basis, solar PV plus batteries can meet 96% of load during June, but only 3% during December, and 67% year-round. This study also analyzes how demand-side management of new food and water infrastructure can aid this objective while providing a constant source of electricity, locally-grown food, and clean water. Findings demonstrate that optimizing the KLRS diesel generator, battery management, and solar energy conversion may reduce diesel generation by up to 100% during June, 31% during the field season (mid-April to early October), and approximately 31% year-round (due to limited solar PV generation during the winter), compared with past operational data.

1. Introduction

Like with other Arctic and sub-Arctic regions across the globe, Canada's northern territories experience some of the highest energy costs in the world. This stems from the need to truck, barge, or fly in diesel fuel to generate electricity, costing over $2.1/L (Canadian dollars (CAD) as of September 2021) in the most remote regions only accessible by plane [1]. To reduce reliance on diesel, solar photovoltaics (PV) have become a popular option since they provide renewable electricity from solar energy during long summer days. For example, the village of Old Crow, Yukon, Canada has saved over $400,000 and 189,000 L of diesel per year by installing a 900 kW solar PV array [1]. Adding energy storage in the form of batteries can extend the use of solar PV electricity into the night; however, upfront capital costs and cold weather are formidable barriers to complete independence from diesel fuel using solar and batteries alone [2]. As communities add technologies to improve food, energy and water (FEW) security, energy demand will only increase [3]. Demand-side management (DSM), or modifying electric load according to intermittent renewable supply, can utilize otherwise excess renewable electricity and consequently reduce diesel generation [4].

The Kluane Lake Research Station (KLRS) in the Yukon Territory of Canada is attempting to become independent from diesel fuel and its high cost of $1.85/L (in 2021). The station is similar in size to a typical village in remote, northern regions of North America (henceforth referred to as "the North"). The station, though, is relatively accessible because it is connected to the continental road system. KLRS is located on the traditional territory of the Kluane First Nation, Champagne-Aishihik First Nation, and White River First Nation of the Yukon Territory. The facility serves hydrologists, ecologists, and glaciologists studying the surrounding watersheds, boreal forest, tundra, and icefield ecosystems. The station is operated by the Arctic Institute of North America (AINA) at the University of Calgary and includes a mess hall, a washhouse, four laboratory buildings, an office building, a headquarters building, and a large cabin. There are ten other small cabins not connected to the microgrid and thus not included in this analysis, as they are powered electrically by individual solar PV systems and heated with wood.

The station's electric energy system is a hybrid solar-battery-diesel microgrid, discussed in more detail in Section 2.1.1. KLRS has also recently installed more sources of electric demand to study FEW security as a living laboratory in the North. This includes a container farm (CF) to grow salad greens and herbs to sell in neighboring communities; and a residential above-ground modular wastewater system, or Sewage Treatment Plant (STP), for the large cabin. KLRS is also considering a water reuse (WR) system for graywater recycling. These technologies are an-

* Corresponding author.
E-mail address: dsambor@stanford.edu (D.J. Sambor).

https://doi.org/10.1016/j.nexus.2023.100200
Received 10 February 2023; Received in revised form 18 April 2023; Accepted 7 May 2023
Available online 13 May 2023

alyzed here as to their potential for DSM and the subsequent impact on reducing diesel fuel combustion. DSM can minimize the effect of renewable resource uncertainty on a microgrid by shifting demand around supply [5].

Whereas substantial literature exists in the field of microgrid and renewable energy optimization [6–9], and many analyses utilize DSM [10–14], there are no studies that optimize DSM of multiple FEW infrastructure loads and energy generation simultaneously in a real microgrid in the North. Some studies analyze container farming and wastewater treatment in isolation; however, a common limitation is that individual loads are not analyzed in sufficient detail to be optimized with DSM [15–18]. For example, Kirchem et. al, 2020, demonstrate in their review article that there are no studies that examine the effect that DSM has on both the operations of water treatment infrastructure and microgrid stability simultaneously [18]. In other words, a balance must be maintained between modifying loads to improve energy management in the microgrid, such as raising thermostat settings of heating water when there is excess solar energy, as well as the effect that changing those loads may have on the infrastructure's ability to serve its purpose, for example ensuring sufficient hot or treated water when demanded. Reviews of field studies of power-to-heat DSM have not demonstrated applications to both small-scale container farming and water treatment [19,20]. Overall, there is a need for DSM studies to consider these new FEW technologies [21], for new indicators quantifying the benefit of DSM in energy islands [22], and for additional field studies demonstrating DSM applications [23]. The specific microgrid settings and controls at KLRS also have not been studied by any existing computer model.

The contribution of this paper is both the development of a novel microgrid energy optimization model for DSM of FEW infrastructure and its real application to an islanded microgrid at KLRS. To our knowledge, no other study has been performed to simultaneously optimize an islanded microgrid in the Arctic/sub-Arctic and then implement findings as part of a living laboratory setting. Thus, this paper addresses calls in the literature for more real applications of DSM in renewable microgrids. The model can optimize diesel generator operation (binary operation and continuous dispatch), solar electricity generation, battery charge and discharge schedules, and the shifting of FEW infrastructure demand with the objective of minimizing energy generation costs. This study builds on prior work analyzing DSM of infrastructure [24,25] and work studying infrastructure across the FEW nexus in indigenous, northern communities [26]. The goal of this paper is to optimize KLRS microgrid operations to reduce costs of diesel fuel, compared with historical costs, using DSM of FEW infrastructure to inform station management how to achieve 100% renewable electricity generation for demand at more hours of the year.

The paper is structured as follows. In Section 2.1, the methods of data collection, modeling, and analysis of each component of the study are discussed, first with an introduction to the station microgrid and then with additional detail of the CF, the STP, and the solar energy system. In Section 2.2, the optimization model is described, and is followed in Section 2.3 by a description of the model simulations to be performed. The results of the simulations are discussed in Section 3, with a focus first in Section 3.1 on optimization of the solar PV, battery, and diesel energy systems without DSM, and then in Section 3.2 considering DSM of FEW infrastructure. Finally, conclusions are made in Section 4, along with a discussion of future work.

2. Methods

2.1. Station Energy Models

2.1.1. KLRS Microgrid

KLRS is powered by its own islanded renewable microgrid and thus not connected to any other regional or continental electric grid infrastructure. A 48.3-kW solar PV array and a 171-kWh lead-acid battery storage system is currently installed, as shown in Fig. 1. The solar array has eight charge controllers, which feed into the battery system. The battery system has four 6.8 kW inverters to satisfy peak station demand, which can reach 20 kW. At an average station demand of 10 kW, the batteries can power KLRS for approximately 10 h. If solar PV cannot meet demand and the battery falls below its minimum state-of-charge (SOC), a 21-kW diesel generator supplies the electric demand. When the diesel generator is operating, it meets load first, and excess generation charges the battery second, until its maximum SOC set point is reached. The generator is capable of ramping to meet any change in demand.

Energy data were downloaded from the KLRS microgrid cloud monitoring system at 10 min intervals (extrapolated from the instantaneous power based on the first data point of each interval) for station electric demand, solar PV generation, diesel generation, and battery charging and discharging. All energy data consist of electricity use connected to the microgrid only, and thus any energy demand met by propane combustion or wood stoves (cooking, hot water, space heating) are excluded from this analysis. The microgrid has been collecting data since February 15, 2020; however, due to the COVID-19 pandemic, the 2020 field season was limited with substantial portions of missing data until a typical field season began in late April 2021.

The normal KLRS field season occurs from mid-April to early October, though it also operates in the winter (offseason) at lower energy demand (Fig. 2). Over the 2021 field season, electricity demand gradually increased as more clientele arrived and the CF was commissioned. On a diurnal basis, power use can be averaged by day, and is shown for select months in Fig. 2.

A majority of the station electricity demand is from the CF, manufactured by CropBox. This is shown in Fig. 3 for a select week in August for the total station electric demand with and without the CF. The CF is discussed in more detail in Section 2.1.2.

Aside from the CF, the station electric demand is from laboratory, office, and communal buildings. There is a baseload of 1-2 kW at all times from information technology (IT) devices, refrigerators/freezers, and laboratory equipment. Additional demand includes water pumping, dishwashing, clothes washing/drying, and office/laboratory equipment.

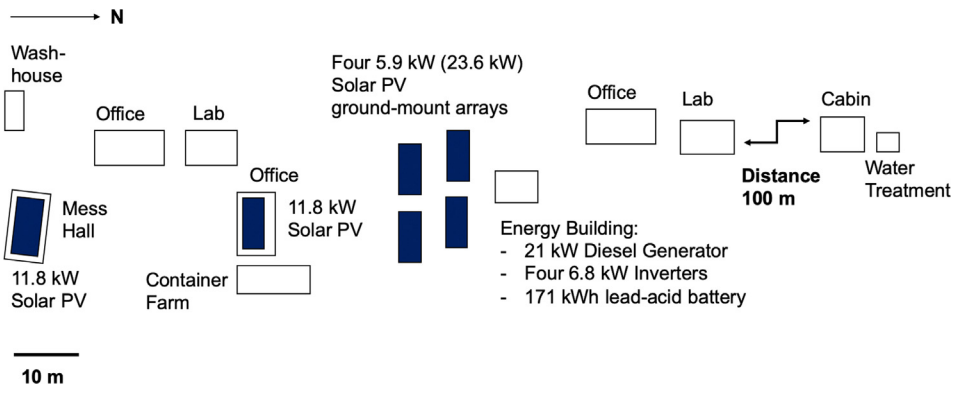

Fig. 1. KLRS microgrid diagram with buildings served and energy systems, with solar PV arrays shaded (two 11.8 kW rooftop arrays and four 5.9 kW ground-mount arrays).

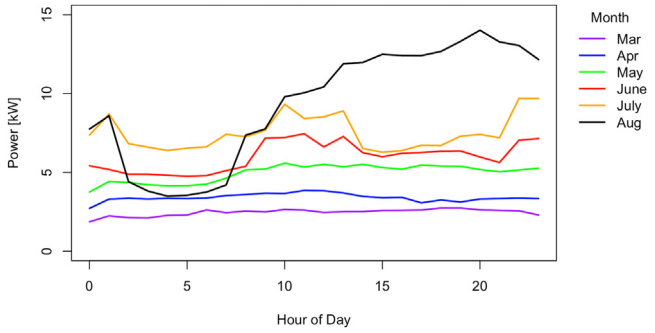

Fig. 2. Average KLRS power use over a day during several months in 2021. The pattern in March is typical of all winter (offseason) months. Energy demand increased over the year as the CF was commissioned to full production.

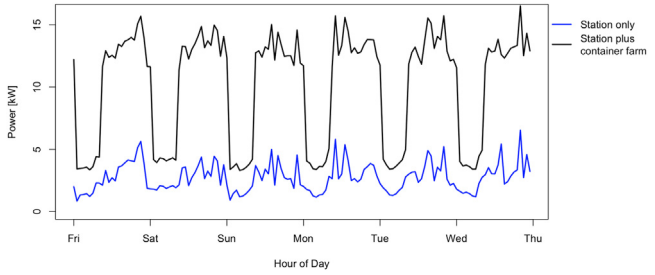

Fig. 3. Electric load for total station demand including the CF, and for station buildings only, over a week in August (Aug 13-19, 2021), plotted at hourly temporal resolution.

Total station power use during the field season is typically 6-10 kW during the day, though it can peak higher during mealtimes and full station occupancy, and 1-3 kW at night. For reference, there is approximately 700 m^2 (7,500 ft^2) of building area responsible for energy consumption on the KLRS microgrid.

The station continues to operate during the offseason through the winter, though at lower power use of approximately 1 kW constant power. Most buildings are closed, except for a large cabin used for winter research and occasional use of the main station buildings. Small kitchen appliances, lighting, equipment charging, and supplementary space heating are typical sources of electric demand. There are occasional peaks to 2 kW for very cold days when supplementary electric heating is used or additional winter research is performed (see Fig. 2 for March, which is typical of winter electric demand).

The station field season is assumed to be April 15 – October 14. However, the station load profile was only able to be analyzed separately from the CF from June 20 to August 24; thus, any analysis of the research station electric demand alone is performed on this time period. The field season electricity use data for the research station (excluding the CF) were clustered into six representative days using k-means algorithms (Fig. 4).

Each day type in Fig. 4 is defined in Table 1. Days 2-3 exhibited lower energy use with a relatively flat shape, given their occurrence in early summer when the CF used less power and less clientele resided at the research station. Most other days had an evening peak, given all clientele would return from daily field work for dinner. Otherwise, peaks in power demand may be attributed to typical times of laundry use. Based on the probability of each day occurring in the time period of collected data, these days were randomly selected to fill periods of missing sections of the station electric load profile.

Table 1
Attributes of representative days of KLRS electric demand.

Name	Percent of Data	Temporal Occurrence	Shape
Day 1	10.5%	Throughout	Mid-morning peak
Day 2	23.0%	Early Summer	Flat
Day 3	26.0%	Early Summer	Flat
Day 4	14.0%	Late Summer	Midday and evening peak
Day 5	16.0%	Late Summer	Evening peak
Day 6	10.5%	Throughout	Evening peak

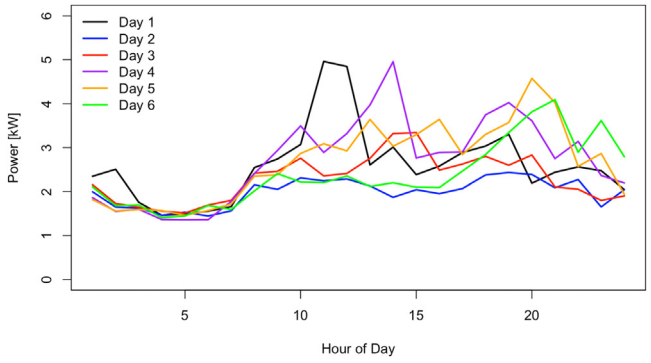

Fig. 4. Six clustered representative diurnal profiles of the station load (without the CF) from June 20 to Aug 24.

2.1.2. Container farm (CF)

CF energy use. The CF energy demand consists of baseload equipment, lighting, and the heating, ventilation and air-conditioning system (HVAC). These three categories are detailed below. The CF operates constantly year-round, with a programmed schedule for equipment and lighting, though with a variable HVAC demand based on weather conditions. Overall, the CF uses on average 8.4 kW of power during the day (lighting on) and 2.5 kW at night (lighting off), for a total of 155 kWh of energy per day (56,590 kWh/year), or the equivalent of five typical homes [27]. Depending on ambient conditions, power demand can peak at 10.5 kW during daytime periods and use 177 kWh per 24 h period. Of this peak power use, 6 kW is attributable to lighting, 2.5 kW for baseload electric equipment, and ~2 kW for HVAC (peak use is for cooling during summer—heating is met by propane). The CF is a standard 40-foot shipping container with a floor area of 12.2 m by 2.4 m and a height of 2.6 m (40 ft x 8 ft x 8.5 ft). The typical interior growing temperature range is 17-21 ˚C; energy optimization of the proper temperature setting within this range is analyzed in Section 3.

Lighting is responsible for a majority of the CF electricity use. Substantial grow lighting is needed because the container is fully opaque and all lighting must be artificial—unlike a greenhouse—given limited sunshine in the sub-Arctic winter. LED strip lighting is used, and despite its relative energy efficiency, the total electric demand is high with four vertical grow shelves. Lighting operates 16 h per day with a power draw of approximately 6 kW. The lighting in the CF is scheduled from 8am to 12am year-round (based on initial commissioning). This schedule is assumed constant for the entire year; however, optimization of this schedule for the purpose of reducing diesel generation is discussed further in Section 3.

Baseload equipment uses approximately 2-2.5 kW of electric power at a fairly uniform, constant schedule over time. This includes a nutrient doser (230 W), water circulation pumps (540 W), dehumidification (850 W), and circulation fans (~200 W). Other loads may operate intermittently, including the water pump feed to the main storage tank runs (90 W for approximately 4 h per day) and an exhaust fan (115 W when lighting is on).

The HVAC system consists of an external fan-coil unit that uses propane heating and electric forced-air cooling, as well as an economizer for cooling when ambient temperatures are less than 10 ˚C. Propane combustion is only needed on very cold winter nights and uses a 400-W electrical fan to blow the hot air into the container; given it is predom-

inantly non-electric, it is not considered for DSM in this study. When lights are on, their 6-kW power draw is a source of substantial internal heat gain that typically triggers mechanical cooling. On warm days with lighting on, the cooling system can operate at up to 2.1 kW of power nearly continuously, or an energy use of 25 kWh/day. Otherwise on mild days, it may run at ~1.7 kW and cycle off for 15 min every two hours, for a total of 20 kWh/day. When ambient conditions are cold enough, the economizer provides cooling using a 260-W fan.

The amount of heating and cooling energy required to maintain proper growing conditions over the year can be modeled based on collected weather data. The amount of heating energy ($Q_{furnace}$) required (propane furnace with electric blower) in each hour on cold days is determined by the heat transfer out of the container via conduction (Q_{cond}) plus any heat loss through exhaust of stale air (Q_{fan}), less any heat provided by internal gains of electric equipment ($Q_{baseload}$). The cooling energy required (Q_{cool}), provided by mechanical cooling, economizer, or exhaust fan, is determined by any heat gain during warm ambient conditions via conduction plus internal heat gains. These thermal energy flows, assuming steady state, in the CF are summarized in Eq. (1) (and discussed in more detail below), which is used to determine the hourly electric demand of the HVAC system for the entire year.

$$Q_{furnace} + Q_{baseload} = Q_{cond} + Q_{fan} + Q_{cool} \quad (1)$$

Conductive heat loss is determined by the UA-value, or heat-loss coefficient, of the container. The UA-value is the product of the U-value (inverse of the R-value), and the surface area (A) of the container. The container insulation is assumed to be R16 for walls, based on typical CF specifications [28]. In this analysis, convective heat loss is included with conductive heat loss by determining a UA-value associated with infiltration, primarily due to air leakage around doors. With infiltration, a total of R13 is assumed for the entire container (radiative heat transfer is assumed negligible).

Other modes of heat loss include running a fan to exhaust hot air from the container, with subsequent make-up air to be replaced and conditioned based on thermostat setpoints. The exhaust fan primarily operates when lighting is on, given that substantial internal heat gains from operating electric equipment can lead to cooling demand even on moderately cold days (assuming all electric energy is converted to heat inside the container). For example, consider September 14, 2021, a moderately cold day with a temperature range of ~0-10°C. The lights turned off at midnight, and the exhaust fan continued to operate to cool the unit to a minimum interior setpoint of 17.4°C. The fan then turned off to keep the container from cooling further. During overnight hours with lighting off, the baseload electric power was 2 kW. With the exhaust fan off, this power draw was sufficient to heat the unit back to 18.1°C, and the exhaust fan turned on again to cool the unit. The cycle repeated until lights turned on later in the morning, which triggered substantial mechanical cooling to balance the internal heat gain.

Using Eq. (1) and weather data, a thermal energy balance model is developed to determine the hourly heating and cooling energy required. A visual example of the model compared with actual operation is shown in Fig. 5. On the warmest days the modeled cooling operation is higher than the actual data. This occurs because the cooling system installed has less capacity than required to cool the container completely. Over the course of a year, mechanical forced-air cooling of the CF is only needed from April to October, and the economizer can provide cooling at other times of year as needed. The model excludes economizer use during the field season given site observation determined that the economizer alone was insufficient to keep the container cool. The CF began full operation in August 2021 after several months of commissioning and variable schedules; thus, this is the only month available for direct comparison between collected and modeled data.

CF energy costs. Based on the data from the 2021 field season and energy modeling of the CF for the rest of the year, the energy operation costs can be compared with the revenues of produce sales. The CF is scheduled to operate year-round at the same produce yield. Produce grown in the CF (namely salad greens and herbs) are primarily sold to neighboring communities, with the remainder consumed on site. During the field season, approximately 15-20% of electric demand is met by the diesel generator, and the rest by solar PV. Meanwhile, in the winter about 90-95% of load is powered by diesel generation. Based on energy costs (discussed in Section 2.2), the cost of operating the CF during the field season is ~$300/month ($0.06/kWh). In a winter month, the CF is modeled to use ~5300 kWh/month and nearly all is met by diesel fuel combustion (~2200 L) for a cost of ~$3300/month ($0.63/kWh). Costs are much lower during the field season given that most of the energy demand is met by solar PV and battery. In addition to fuel costs, there is also an operations and maintenance (O&M) cost of approximately $2400/year or $200/month to run the diesel generator.

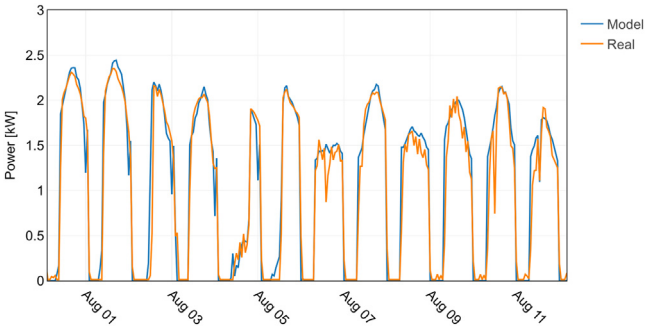

Fig. 5. Example time period in late summer (July 31 – August 12, 2021) of modeled forced-air cooling operation compared with real cooling operations from collected data of the CF.

Produce can sell at $40/kg ($18/lb), or ~$800 total per weekly harvest. In the summer, energy costs are small due to high solar PV production and low diesel generation, or only 15% of revenue. However, in the winter with minimal solar generation, the cost of operating the CF is nearly equal to the revenue of harvests. The total costs of a summer month and winter month of food production are shown in Table 2 (with spring and fall lying in between the two extreme cases).

2.1.3. Wastewater treatment

This study analyzes two forms of water treatment systems at KLRS using DSM. One is a residential above-ground modular sewage treatment plant (STP) that is currently in operation for blackwater and graywater treatment with disposal to the landscape. The other is a water reuse (WR) system for recycling graywater that may be installed in the future. These two systems are discussed below.

The STP has been installed at the large cabin on-site used year-round. Graywater and blackwater from the cabin drain into a lift station holding tank. The sewage is then pumped, operated by a float switch, to the STP system, capable of treating 1,135 L/day (300 gal/day). It enters a sedimentation chamber and then a main treatment chamber, where an aerator provides oxygen for bacteria. Ultraviolet (UV) light then disinfects the water. An effluent pump, also controlled by a float switch, pumps the water out periodically (in this case to an existing outhouse holding tank). Given the short duration of operation, the pumps use a

Table 2
Relevant costs for operating a CF at KLRS including diesel fuel and O&M cost for electricity generation to grow a variety of produce (salad greens and herbs) in 2021.

Season	Fuel Cost ($/mo)	O&M Cost ($/mo)	Total Energy Cost ($/mo)	Energy cost of produce ($/kg)
Summer	300	200	500	6.25
Winter	3,300	200	3,500	43.75

Table 3
Electric loads within a STP modular sewage treatment plant.

Load	Power (W)	Time per day	Energy Use per day (kWh/day)
Lift Pump	400	5 min	0.0
Lift Heat Trace	400	As needed	To 10°C setpoint
Aerator	46	24 hr	1.1
Main Heat Trace	400	As needed	To 10°C setpoint
UV Lamp	40	24 hr	1.0
Controls	10	24 hr	0.2
Effluent Pump	400	5 min	0.0

negligible amount of energy. These loads are shown in Table 3. There is an average baseload power of 125 W, or 3 kWh/day.

Heat trace must be used during the winter in the lift station and STP unit to keep the water from freezing and enhance aerobic bacteria functions. The thermostat setpoint is 10°C. This setpoint will be subject to DSM in this study to optimize use with renewable energy (Section 3.2). Heating season is approximately aligned with the field season at KLRS, when the average temperature is below 0°C from mid-April to early October (Fig. 6).

A thermal model can be developed for the STP system to determine electrical energy required for the heat trace. The STP system is a 1.5 m by 2.4 m box with a height of 1.5 m. The unit sits on a platform frame to avoid ground thaw; thus, heat loss occurs via conduction and convection from all sides to the ambient air. The lift station is a 1.1 m diameter and 1.2 m high cylinder, partially buried into a gravel pad; therefore, only conductive heat loss is assumed given snowpack would likely insulate it from the air above.

The combined heat loss rate (q_{loss}) is proportional to the total UA-value and the temperature difference between the unit interior and the ambient (Eq. (2)). Heat loss is assumed to be only through conduction and convection, and infiltration can be neglected given the system is tightly sealed. Granted, fresh air from the aerator must be heated and humidified from the cold, dry ambient; however, thermal gains from the electric equipment and humid environment inside the STP approximately offset this heat loss. Wastewater from the house is also relatively warm and provides additional thermal gains.

$$q_{loss} = U A(T_{in} - T_{amb}) \tag{2}$$

In the most extreme case with an ambient temperature of -50°C, the heat loss is ~300 W each for the STP and lift station. Therefore, the heat trace rated at 400 W and installed in each should be sufficient, with a maximum of 800 W if both are operating simultaneously (though typically run in alternating mode).

Thus, the typical power draw of the entire system in the heating season would be 925 W, with a baseload of 125 W and occasional pump power spikes for one-minute intervals. The energy demand for non-heating electric loads is modeled to be 1115 kWh/yr (~3.1 kWh/day) and the total energy for heating (met by electric heat trace) is 391 kWh/yr (~2.2 kWh/day during the 181-day long heating season from

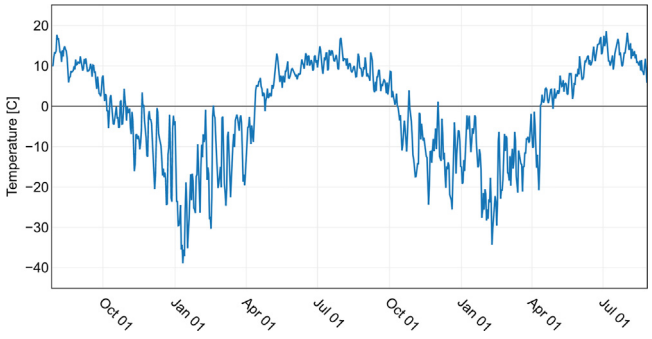

Fig. 6. Average daily temperature (°C) from July 2019 to Aug 2021 at KLRS.

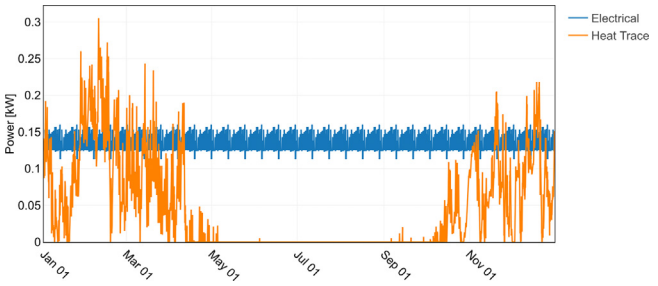

Fig. 7. Hourly power demand for the STP system including the lift station, separated between electrical components (aerator, UV, pumps), and electric heat trace over a year.

October 6 to April 11), as shown in Fig. 7. So, in winter with primarily diesel generation, the STP would cost $3.29/day to operate.

The STP also has significant thermal mass associated with water storage that can allow for variable setpoints in order to utilize DSM; this will be subject to optimization in Section 3.2. The STP has a capacity of ~2500 L (670 gal) and the lift station can store 379 L (100 gal). Given the high specific heat capacity of water, the system has a total thermal capacitance of 3.4 kWh/°C.

KLRS is also interested in installing a WR system at the same cabin in order to recycle graywater. The WR system has been developed at University of Alaska Anchorage and is a modular system capable of treating up to 227 L (60 gal) per day of domestic wastewater from sinks, showers, and laundry to be reused for these purposes [29,30]. The main treatment processes consist of cartridge filtration, nano-filtration, and reverse osmosis, which each draw about 400 W of electric power. Along with supplementary processes, including UV and ozone treatment, the system uses on average 3.4 kWh/day. Space heating of the 10-foot shipping container that houses the system and domestic hot water heating each draw about 1 kW of power and 2 kWh/day in the winter. Given there are water storage tanks in between each treatment process, the treatment processes can be dispatched using DSM, subject to treatment processing and water storage constraints. Heating can also be dispatched by varying thermostat settings for the container and the hot water tank. Optimization of these processes is discussed in Section 3.2. For more detail of the WR system processes and constraints, please see Sambor et al. [24].

2.1.4. KLRS solar and weather model

KLRS has a total of 48 kW (DC, rated peak power) of solar PV installed. Approximately half (24 kW or 64 modules) are Hanwha Q.Peak 370-W panels and the other are Canadian Solar 385-W panels. Half of the solar PV capacity is ground-mounted and the other half is roof-mounted. There are four 5.9-kW ground-mount arrays, or two arrays of each type of panel. The ground-mounted arrays face due south (azimuth of 180°) with a tilt of 35°. The roof of the mess hall has 11.8 kW of solar PV (four strings of 8 Hanwha panels) and the operations building has the same array but of Canadian Solar PV panels. Both rooftop arrays are tilted at 15°, though the mess hall roof has an azimuth of 220° and the operations building roof has an azimuth of 190°.

Weather data were collected at an on-site weather station for shortwave solar irradiance (W/m^2), temperature (°C), and snowpack thickness (relevant for modeling reflected solar irradiance). Electricity generation was modeled given that collected solar generation data also accounts for substantial curtailment when the battery is full, thus not representative of potential generation. Typical meteorological year (TMY) data does not account for the fact that the Kluane Ranges to the south block all direct solar irradiance (albeit weak) between late October and mid-February.

To determine the irradiance striking the tilted collector surface, the station pyranometer data for global horizontal irradiance can be approx-

imately divided into beam irradiance (direct rays) and diffuse irradiance (scattered rays from clouds and surfaces). The percentage of global irradiance that is diffuse irradiance can be approximated to be proportional to beam irradiance based on a diffuse sky factor, as shown in Eq. (3) [31], where n is the day number of the year.

$$C = 0.095 + 0.04 \sin\left[\frac{360°}{365°}(n - 100)\right] \tag{3}$$

It is assumed that when the solar altitude angle is below 15°, or between October 25 (day of year: n = 299) and February 15 (n = 46), all radiation is diffuse. The diffuse sky factor can then be used to determine the approximate proportion of global irradiance that is beam versus diffuse irradiance.

The amount of diffuse irradiance that a tilted collector obtains is a fraction of the total horizontal diffuse irradiance because it only faces a portion of the sky, as defined in Eq. (4) by the tilt angle (θ).

$$I_{d,tilt} = I_{d,hor}(1 + \cos\theta)/2 \tag{4}$$

The beam irradiance on a collector surface can be determined using geometric relationships based on the altitude angle of the sun, the azimuth angle of the sun, and the tilt of the collector surface. The altitude angle (β) is defined by Eq. (5), where ϕ is the latitude (61° for Silver City, Yukon).

$$\beta = 90 - \phi + 23.45 \sin\left[\frac{360°}{365°}(n - 81)\right] \tag{5}$$

The beam irradiance on the collector surface can then be expressed in Eq. (6), where ϕ_c is the azimuth angle (orientation) of the collection surface with respect to south (0°) where east of south is positive.

$$I_{b,tilt} = I_{b,hor}(\cos\beta\cos\left(0 - \phi_c\right)\sin\theta + \sin\beta\cos\theta)) \tag{6}$$

In a snowy climate like the Yukon, the reflected solar irradiance off snowpack can also increase the total irradiance on a collector surface. The reflected irradiance is given by the reflectance, the total horizontal irradiance, and the fraction of reflected irradiance available given the collector tilt angle, as shown in Eq. (7), where the reflectance (ρ) is 0.8, assumed only for when the weather station records a snowpack greater than 2 cm. Increased reflected irradiance is only available to the ground-mount arrays and not the roof-mount arrays.

$$I_{r,tilt} = \rho(I_{b,hor} + I_{d,hor})(1 - \cos\theta)/2 \tag{7}$$

Finally, solar modules lose power if they increase in temperature. Thus, ambient temperature data from the weather station was used to calculate the cell temperature of the Hanwha and Canadian solar PV panels, as in Eq. (8), where *NOCT* is the nominal operating cell temperature, rated for each panel (Table 4).

$$T_{cell} = T_{amb} + \frac{NOCT - 20}{0.8} \tag{8}$$

At the site, it is predicted that the hottest cell temperature for the Canadian Solar module is 53.7 °C and for the Hanwha panels a maximum temperature of 57.4°C. When the cell temperature is above 25 °C, this reduces the power production below the theoretical maximum, per Eq. (9), where P_{loss} is the percentage of power reduction per °C above 25 °C, which is different for each panel (Table 4).

$$P_{DC} = P_{DC,rated}\left[1 - P_{loss}\left(T_{cell} - 25\right)\right] \tag{9}$$

Temperature losses account for 10.3% reduction at the hottest time of year for the Canadian Solar panels and 12.6% reduction for Hanwha panels. The effect of wind speed on cell temperature can be neglected due to relatively low wind speeds during summer at KLRS.

Table 4
Specifications of the solar PV modules at KLRS.

Solar Module	NOCT (°C)	P_{loss} (%/°C)	Efficiency (%)
Canadian	42	0.36	18.6
Hanwha	45	0.39	19.4

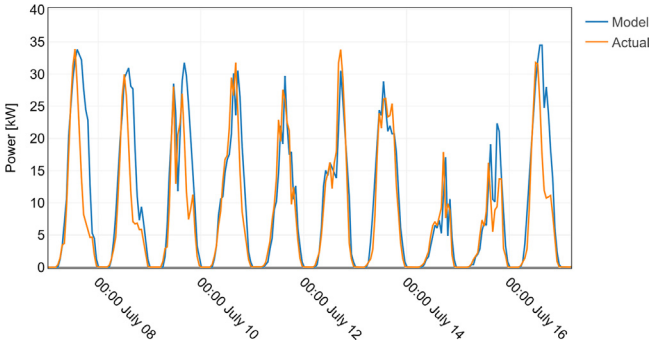

Fig. 8. Solar generation model versus actual solar energy used at KLRS for a week in July at hourly resolution.

Each solar PV array at the station can be modeled to determine the final DC power available based on the total collector solar irradiance, and then aggregated among arrays. A conversion efficiency of ~95% to account for inverter losses is assumed in order to provide AC power to the station. A qualitative evaluation of the model (Fig. 8) for a random week in July 2021 compares modeled solar production with actual solar generation absorbed by the microgrid. Note that there is a disparity during afternoons with high solar resource because, in actual operation, solar generation had been curtailed when the battery reached full capacity in the late afternoon; thus, a direct quantitative evaluation is not possible because curtailed energy is not measured. The question of how to minimize curtailment is addressed in Section 3.1.

This qualitative comparison is similar for the rest of the field season. To be clear, solar generation is nearly negligible from late October to mid-February. Data collection is ongoing at KLRS for further model validation with pyranometers installed at the plane of the solar arrays in late August 2021. Additional ground-mount solar PV may be installed in the future; however, many other innovative solar PV options, such as floating PV (FPV) or agrivoltaics, would prove too challenging to install given the long, severe winter at Kluane Lake.

2.2. Optimization model

An optimization model has been developed to determine how KLRS can reduce diesel fuel use compared with historical operation through optimal microgrid management of solar PV, battery energy storage, and DSM strategies. The model is mixed-integer linear developed in Julia/JUMP (Version 1.1.0) at an hourly temporal resolution [32]. The model inputs hourly annual profiles of electric load demand at the station, including the CF and STP, as well as weather inputs, assuming a perfect forecast (see Appendix A for all model inputs). The model has purposely been simplified to improve computational speed and allow for application to other communities in the North.

The model optimizes three groups of decision variables: (1) hourly dispatch of energy generation (solar energy to curtail, diesel dispatch power (G_t), and diesel binary variable (D_t); (2) battery storage management (hourly charging and discharging with associated state-of-charge); and (3) hourly DSM of dispatchable loads (amount of heating for sewage treatment, WR system dispatch, and cooling of the CF with temperature control).

The model objective is to minimize total diesel generator costs associated with powering the station, summed over each hourly time step (t), in present Canadian dollars, as shown in Eq. (10).

$$\min \sum_t C_G\, G_t \;+\; C_{OM}\, D_t \mid D_t \;-\; D_{t-1} \mid C_d \tag{10}$$

Diesel generator costs include fuel costs of $1.59/L ($6/gal), O&M costs of $2 per hour of generator runtime, and start-up/shut-down costs

(C_D) of \$0.16 per event, based on costs from September 2021. The effective cost of diesel-generated electricity is \$0.67/kWh (C_G) plus \$0.10/kWh (C_{OM}) O&M cost for a total of \$0.77/kWh, based on a 2.4 kWh/L generator fuel efficiency. O&M costs for the solar PV and battery energy storage systems are negligible based on an agreement between the solar installer and the research station for lifetime warranty service.

The objective is subject to standard constraints on energy flow balance as well as generation, storage, and load capacity limits. Of particular note here are the constraints that diesel generation must turn on at a battery SOC minimum level (SOC_{min}) and turn off at a maximum level (SOC_{max}) in Eqs. (11) and (12), respectively.

$$D_t + SE_t / \left(E\left(SOC_{\min}\right)\right) < 1 \tag{11}$$

$$D_t + SE_t / \left(E\left(SOC_{\max}\right)\right) < 2 \tag{12}$$

Where SE_t is the stored energy in battery at time step t, and E is the battery storage capacity. Also of significance is a finite-difference temperature (T) constraint to allow for optimizing the amount of heat or cooling (Q) to provide for DSM programs in the CF, STP, and WR system container and hot water tank, as shown in Eq. (13).

$$T_{t+1} = T_t + (1/C)\left[\eta Q - UA\left(T_t - T_{amb}\right)\right] \tag{13}$$

Where C is the thermal capacitance of either the structure or water stored, UA is the heat loss coefficient of the respective thermal envelope, and η is the efficiency of the heating/cooling systems. Complete model mathematical form is shown in Appendix A. The two different parts of the optimization procedure and their respective time periods of inputs and outputs are discussed in the following section.

2.3. Simulations

The first section of the modeling procedure is to analyze the current operation of the station microgrid without DSM. The results of this set of simulations is discussed in Section 3.1. The model simulations are performed only for four individual months of the year (May 3 – August 24, 2021), given the authors were only able to reside and collect the station during this time period for the most reliable comparison. Energy data, collected at 10 min intervals and summed to hourly intervals, included total station electric demand and diesel generation, solar generation, and battery discharge to meet this demand as well as electricity generation for battery charging. In the status quo, the microgrid operates by utilizing solar generation directly to meet load and using any excess generation to charge the battery. Otherwise the battery meets load until its SOC reaches a minimum setpoint, then the diesel generator operates to meet load and raise the battery SOC to a maximum setpoint, and the generator is turned off. At the start of the field season, the minimum and maximum setpoints were 60-80%; changing these parameters is discussed in Section 3.1.

In this first section of simulations, the model is used to optimize how the diesel generator should operate as well as battery dispatch with available solar generation. In this way, the optimized case can be directly compared to the actual data. Granted, the model performs with perfect forecast; while the results presented are thus an optimistic estimation of savings, the authors noticed that their own forecast at least for day-ahead weather conditions for predicting solar irradiance were rather accurate based on knowledge of the local microclimate. Computational time varied from approximately one hour to a day, mainly relative to the amount of diesel generation required to balance load.

The second section of the modeling procedure is for optimization of the entire microgrid including DSM. This analysis is performed in Section 3.2. The model is used to analyze dispatchable load integration by incorporating models of how each load (CF, STP, and WR system) would have performed differently had their operations been optimized (e.g. controlling thermostat settings), in addition to optimizing energy generation and storage. Given the water treatment systems were not yet in operation and the CF was not yet suitable for DSM, this is a more hypothetical analysis compared to the first section of simulations.

The optimization is compared to actual microgrid operations data for the time period above (May – August 2021), and collected plus modeled data was used to form an entire year (September 2020 – April 2021). The dispatchable FEW loads were initially modeled for operation in the status quo (i.e. constant thermostats). Some time series data during the off-season had substantial missing data that required modeling to fill gaps. This was done by repeating prior or subsequent sections of collected data; this procedure for missing data was deemed appropriate because the off-season demand is relatively constant. Based on available data and computational capacity, models for different months were run at different temporal resolutions: weekly periods (January – March and September) and four-day periods (October – December). In order to determine these periods, four representative days per month were clustered using k-means algorithms; the representative days were chosen to fill the modeling time period based on their likelihood to occur in the given month. Clustering by diurnal periods was deemed appropriate given there is no optimization of capacity variables, and battery storage cycles are confined to approximately a day of station operation. This modeling procedure also reduced computational capacity required to solve the optimization.

Two sub-sections of simulations are performed in this second section (Section 3.2): in the Base Case, modeled dispatchable load profiles are fixed, and then in a Dispatchability Case, the model can optimize how each of the technologies would operate using DSM. The specific loads are seasonal with respect to their flexibility: the CF cooling dispatch season aligns approximately with the field season from April to September, the STP heat trace is off during the field season from May to September, and the WR system is assumed to operate year-round.

3. Results and discussion

3.1. Microgrid energy system optimization

The optimization model is used to determine how much diesel fuel can be saved if the microgrid energy generation and storage systems were optimized to utilize as much solar generation as possible, compared with actual operations data. In this simulation, the generator dispatch, solar PV generation, and battery charging/discharging can be optimized. Results are shown for the 2021 field season in Table 5.

After modeling and analysis of microgrid operations during experimentation on site May – July, 2021, simulations were performed to determine a more optimal battery SOC range for diesel generator charging. It was observed that substantial diesel fuel was used and solar energy

Table 5
Monthly model runs of actual versus modeled KLRS microgrid dispatch.

	Actual			Model		
Month	Diesel (kWh)	Diesel Operation(h)	Solar (kWh)	Diesel (kWh)	Diesel Operation(h)	Solar (kWh)
May	169	18	4,010	22	2	4,125
June	8	2	5,008	0	0	4,875
July	605	71	5,865	327	19	5,877
August	1,735	141	3,548	1,383	67	4,534

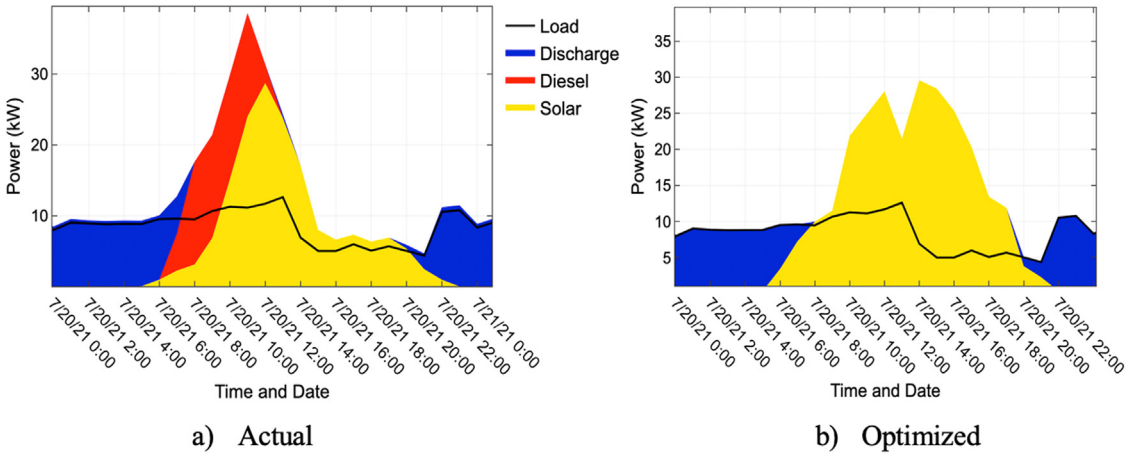

Fig. 9. Actual KLRS operations data for July 20 (left) versus optimized microgrid dispatch with no diesel generation. Discharge means energy from the battery to meet load.

curtailed because the generator had already charged the battery to a high setpoint by the time of day when solar resource was high. Based on modeling, the SOC range was changed on site from 60-80% to 40-60% in August 2021, in order to leave more battery capacity available for solar charging while maintaining the same 20% SOC range for diesel charging. The results of comparing actual to optimized hourly operations of the microgrid demonstrate that in July, the percent reduction in diesel energy was 46% and in August it was 20%. Similarly, in July the percent reduction in diesel operation hours from historical operations to the optimization model results was 73%, and in August it was 52%. This demonstrates that the new SOC range was more effective at reducing fuel given the optimization model had less of an effect in decreasing diesel use. The effect of this change on a daily basis can be seen in Fig. 9.

Over the 2021 field season, diesel would be reduced by 31%, or approximately 327 L, if optimally controlled compared with past data. Granted, the model has perfect forecast and thus savings in reality would be less, though solar cloud forecasters in weather models have improved in recent years [33]. In the model, 62% fewer hours of diesel run time would be required or 144 fewer hours total. During this time, the total electric demand was 19,141 kWh, 13% of which was met by diesel in actual operation. If optimized, 9% of load would be met by diesel. A sample day in July contrasting the differences in microgrid dispatch between actual and optimized microgrid dispatch is shown in Fig. 9.

In Fig. 9, all energy generation above load is either charged to the battery or curtailed. In the actual historical data (Fig. 9a), curtailed solar is already included in solar generation data, hence the steep decline in solar generation during early afternoon on an otherwise sunny day. This occurred because the generator turned on at 6am when the battery SOC fell to 60%, then the generator powered the station and charged the battery to 80%, and finally the generator turned off at 12pm. Solar PV, on a high solar resource day, then charged the battery to 100%, while most of the day's subsequent solar PV generation was curtailed. In the optimized case (Fig. 9b), the battery dispatch is optimized such that the battery SOC did not decline to the minimum setpoint and thus did not trigger the generator to turn on in the morning, thus allowing the solar PV to charge the battery completely to 100% by evening.

Overall, simply by understanding patterns in load and operating the diesel only as much as necessary, KLRS could get substantially closer to its goal of 100% renewable energy during the field season. With optimization of the microgrid, KLRS could operate at 100% solar PV generation for the month of June. This analysis is only performed for the field season given the availability of quality data with which to compare to actual operations; limited improvements can be expected during offseason months.

3.2. FEW infrastructure demand optimization

The operation of FEW infrastructure components as dispatchable loads can be analyzed for further diesel savings. Given the collected historical data are not broken down by individual load, the electricity use of each dispatchable load must be modeled for an entire year. Then this modeled load profile is removed from the collected load data so that its operations can then optimally be added back in by the computer model.

The optimization is performed first using the modeled profile without DSM (Base Case). In other words, heating and cooling systems are assumed to have fixed thermostat setpoints. Then, the load profiles for each dispatchable load are removed from the total load profile and optimally dispatched back in (Dispatch Case). Dispatch is performed with respect to constraints: the CF thermostat is allowed to vary from 17 to 21 ˚C for cooling, and the STP thermostat from 10 to 21 ˚C for heating. The simulations are performed for each month and presented in Table 6.

Allowing CF cooling and STP heating to be dispatched flexibly using DSM results in modest reductions of diesel generation. The Base Case has been optimized with respect to energy generation and storage compared with the collected data. Then in the Dispatch Case, DSM is allowed to optimize the select loads, though these loads are small compared with the entire microgrid. Over the annual time horizon, diesel fuel use is reduced slightly by 27 L and runtime is reduced by 14 h for a cost savings of $70. However, a more substantial reduction of 6% in solar curtailment occurs due to flexible load dispatch. The cooling system for the CF, while a large load at 2 kW, already occurs mostly during solar hours and in the summer when diesel use is limited. STP heating occurs during the winter when diesel use is predominant, though it is a smaller load of less than 0.5 kW.

Other than fuel savings, there are notable changes to microgrid operations when the optimization model is applied. In April, the STP sewage treatment system is dispatched much more during the daytime to take advantage of otherwise excess solar energy, than if the thermostat was fixed. This is shown in Fig. 10 with the STP heat line (purple) above the base load profile (black). If the thermostat is fixed, only small increments of heating are called for during the day, resulting in substantial amounts of solar curtailment. The case of flexible dispatch allows for storing the solar energy as heated water, as opposed to storing in a battery or curtailing.

The effect of having a dispatchable setting can also be analyzed with respect to battery storage levels. Over the course of a day in April (Fig. 11), the STP heating system did not start because it acquired enough heat in the prior period to coast down in temperature without reaching the minimum thermostat setting. In the Base Case, however,

Table 6
Monthly simulations of fixed thermostat (Base Case) versus flexible thermostat (Dispatch Case) optimization for STP heating and CF cooling.

	Base				Dispatch			
Month	Total Energy Cost ($)	Diesel (kWh)	Diesel Operation (hrs)	Curtail (kWh)	Total Energy Cost ($)	Diesel (kWh)	Diesel Operation (hrs)	Curtail (kWh)
Jan	2,053	2,667	128	0	2,050	2,666	128	0
Feb	2,958	3,834	188	0	2,951	3,835	184	0
Mar	1,771	2,290	112	66	1,767	2,286	112	66
Apr	351	448	24	158	330	421	23	115
May	373	471	27	518	370	468	26	501
June	191	243	13	1,330	189	240	13	1,266
July	3,026	3,921	196	408	3,022	3,915	196	389
Aug	1,337	1,717	89	260	1,333	1,709	89	248
Sep	3,390	4,397	214	0	3,386	4,389	214	0
Oct	4,100	5,301	264	0	4,092	5,309	256	0
Nov	3,455	4,472	218	0	3,450	4,467	218	0
Dec	4,243	5,515	264	0	4,238	5,507	264	0
TOTAL	27,248	35,276	1,737	2,740	27,178	35,212	1,723	2,585

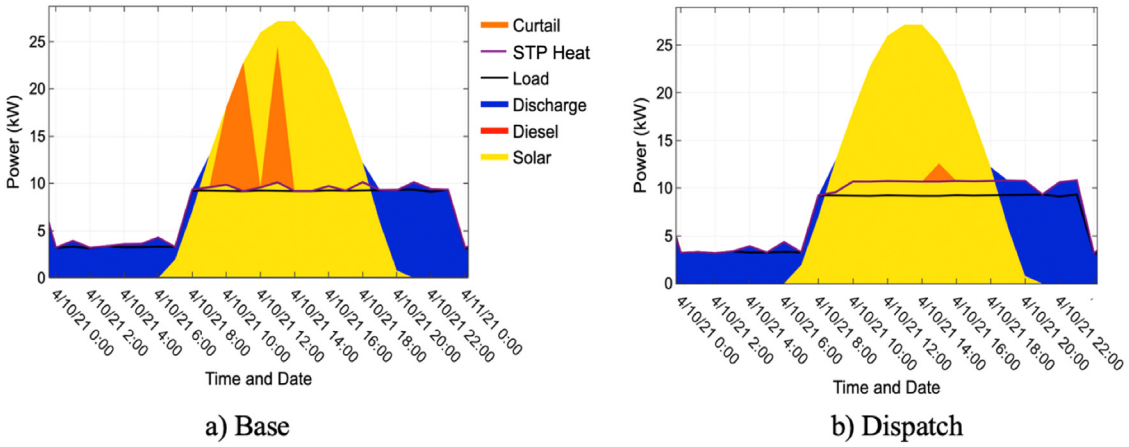

Fig. 10. Optimized microgrid dispatch profiles of energy supply and demand, for a) Base Case with a fixed thermostat for the STP system and b) Dispatch Case with flexible heating.

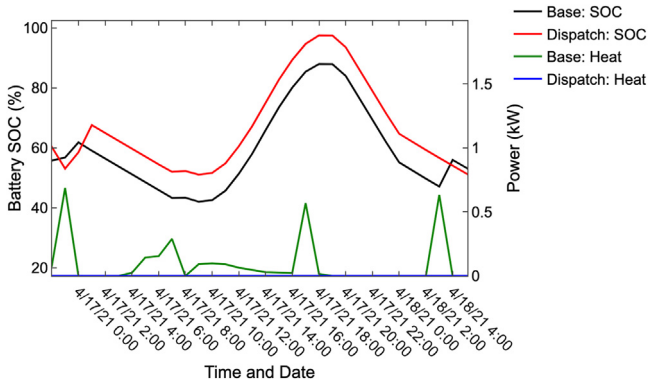

Fig. 11. Comparison of power used for STP heat trace between the Base and Dispatch cases on April 17 with associated battery storage state of charge levels.

the unit must regularly turn on to heat since it is only programmed with a fixed thermostat setting. In the following early morning period (in the Base Case), the battery storage level hits a minimum threshold and triggers the generator to turn on. Conversely, given the flexible dispatch schedules in the Dispatch Case, there is sufficient battery energy storage so that the generator does not start. Instead, the microgrid can wait until there is sufficient solar energy to charge the battery (Fig. 12). Thus, DSM can ensure microgrid operations using 100% renewable energy for several days at a time with sufficient solar resource.

Dispatching the cooling system in the CF results in similar electricity use patterns. For example, on June 1, a day with abundant, excess solar resource, the model in the Dispatch Case curtails 3 kWh less solar compared with the Base Case. This otherwise wasted solar generation is used to cool the container below the normal thermostat setpoint by 3°C so that it is pre-cooled before solar resource declines in the evening, and less cooling is demanded when there is less solar energy.

Adding a WR system to the KLRS microgrid to recycle graywater can also be examined. In the Base Case, a WR system, without any DSM, is added to the KLRS microgrid. In May, operating a WR system would add 130 kWh of diesel generation and 5 h of diesel operation time while increasing energy costs for the month by 20%, as opposed to not installing a WR system. However, if the WR system's treatment and heating processes can be dispatched flexibly, then only 80 kWh of diesel use and 3 h of diesel operation time are required, while increasing the monthly energy cost by only 14%. Overall, dispatching the WR system processes, as opposed to default fixed schedules, reduces diesel energy by 53 kWh and diesel operation time by three hours per month. Results are similar in other field season months.

The ability to operate the container farm and water treatment systems depends strongly on the cost of energy required to power them. As energy prices increase, it may be prohibitive to grow food or treat water, and the infrastructure may not be used in favor of the status quo. Thus, the integration of renewable energy to reduce energy costs, compared with diesel generation, has an effect on the ability to provide food and water, as part of a broader FEW nexus. The results demonstrate that optimizing FEW infrastructure operations can also reduce energy costs

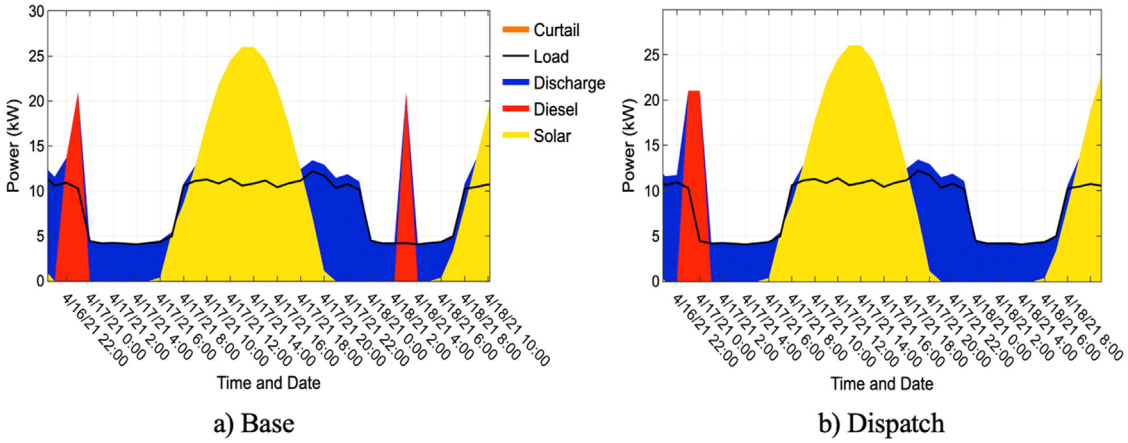

Fig. 12. Microgrid dispatch on April 17-18 in a) the Base Case with diesel generation, and b) Dispatch Case with less frequent diesel generation required.

and thus contribute to the community's ability to utilize them to address FEW security.

To be sure, adding new FEW technologies to improve FEW security will increase total electric demand. Electricity is expensive and any new infrastructure loads would increase energy costs. However, if new electric loads are dispatched to run when renewable energy is in excess, to the extent possible, then the total load can be much smaller than anticipated. This also frees storage capacity in the battery to be used for non-dispatchable loads, without requiring a larger battery to integrate new FEW electric loads. This study may assist KLRS and other community decision-making processes about tradeoffs across the FEW nexus.

4. Conclusion

Overall, with microgrid dispatch optimization, KLRS can substantially reach its goal of 100% renewable energy during several months of the year without any additional energy infrastructure needs beyond the solar and battery system it already has. For the month of June, the station can operate with 96% of energy generation from solar PV and storage with batteries, and 100% with such generation and storage using DSM of FEW technologies. Annually, solar PV and batteries can meet 67% of load. Optimizing battery storage levels and diesel generator operation to maximize solar use for the past field season can reduce diesel fuel use by 31% annually and the total hours of diesel generator runtime by 62% annually. Dispatching loads optimally using DSM of a CF and STP can reduce total annual solar curtailment by 6%. Note that nearly all of the aforementioned savings occur during the half of year when the northern hemisphere is tilted towards the sun (approximately late March to late September), as there is limited solar PV generation in the North during the winter.

As is often the case in islanded microgrids, installing the last amount of renewable generation and storage to get to 100% renewable energy is often not cost-effective if the microgrid already has a high percentage of renewable generation. This study demonstrates that DSM can be the most affordable means of achieving the final goal of 100% renewable generation and use by allowing turning diesel generators off while not requiring additional solar PV and battery storage capacity. In remote areas, utilizing existing infrastructure to provide DSM, as opposed to shipping and installing new generation and storage technology, may also prove to be much easier and cheaper.

Select results have also been implemented in practice at KLRS over the past field season. Optimal microgrid settings and controls, such as battery DOD, generator start/stop settings, and lighting schedules in the CF, have been recommended by this study and incorporated into KLRS operations by staff to validate some of the modeling presented here. The effect of changing the loading and capacity of the diesel generator is also being analyzed for future work. Full implementation of DSM programs and their effect on the plant growth and water quality, for example, can be continued in future work. KLRS offers a unique perspective as a living laboratory and representative "community" of the sub-Arctic. This model can be used for integrating generation and dispatchable load technologies in other communities across the sub-Arctic and Arctic, and potentially in other remote communities worldwide.

Funding

This work was supported by the United States National Science Foundation [Award No. 1740075: IN-FEWS/T3: "Coupling Infrastructure Improvements to Food-Energy-Water System Dynamics in Small Cold Region Communities: MicroFEWs"] Partial funding was also provided by the U.S. Army Corps of Engineers Engineer Research and Development Center (ERDC) under Federal Award Identification Number W9132T2220006.

Declaration of Competing Interest

The authors declare that they have no known competing financial interests or personal relationships that could have appeared to influence the work reported in this paper.

The authors declare the following financial interests/personal relationships which may be considered as potential competing interests:

Data availability

Data will be made available on request.

Acknowledgments

The authors would like to acknowledge Richard Wies, Erin Whitney, and the KLRS staff for their support of this research.

Appendix A

KLRS Model Formulation

The Appendix is presented here as supplementary information for the optimization model used to study the KLRS microgrid.

A.1. Nomenclature

- KLRS: Kluane Lake Research Station
- DSM: Demand-side Management
- FEW: Food-Energy-Water
- CF: Container Farm

- STP: Sewage Treatment Plant
- WR: Water Reuse

A.2. Model inputs

Microgrid Inputs

- Station Electric Load profile (L) [kW averaged in each hour: kWh], including:
  - Container Farm Electric Load profile [kW averaged in each hour: kWh]
  - STP Electric Load profile [kW averaged in each hour: kWh]

Weather Inputs

- Ambient Temperature profile (T_{amb}) [°F]
- Solar Insolation profile [kW_{AC} in each hour per kWp installed, includes losses]

Economic Inputs (all in CAD)

- Total Diesel Fuel Cost: $1.59/L (~$6/gal)
- Diesel O&M: $2/hr
- Start-up/Shut-down Cost: $0.16/step (5 min per step of O&M)

Generator Inputs

- Capacity: 21 kW
- Minimum Loading: 30%
- Fuel Efficiency: 2.4 kWh/L (9 kWh/gal) (based on historical operation)

Battery Inputs

- Battery Depth-of-Discharge (DOD): 60% (171 kWh total, initially at 60% SOC)
- Battery Round-Trip Efficiency: 88% (94% charging and discharging efficiencies)
- Battery Self-Discharge Rate: 0.03%/hr (~2-3%/month)

Solar Inputs

- Solar: 48.3 kWp DC
- Solar Charge Controller / Inverter Efficiency: 95%

Container Farm

- Container Size: 2.4 m x 12.2 m x 3 m (8 ft x 40 ft x 10 ft)
- Container Insulation: R13 [1/(Btu/hr-ft^2-°F)] (UA=122 Btu/hr-ft^2-°F)
- Cooling EER = 11 Btu/Wh

A.3. Model outputs

- Dispatch Scheduling
  - Time series of solar utilization
  - Time series of diesel dispatch
  - Time series of diesel on/off operation
  - Time series of charging/discharging of battery
  - Time series of amount in storage
  - Time series of CF HVAC and STP heat trace
- Total Energy Output (kWh)
  - Total diesel energy generation and fuel use
  - Amount of renewable energy utilized
- Costs
  - Total cost of diesel fuel
  - Total O&M cost
  - Total warm-up/cool-down cost

A.4. Condensed mathematical form

- Energy Supply/Storage Decision Variables
  - Dispatch time series of battery energy storage (charge and discharge) and subsequent storage level
    - $E^{in/out}{}_t$, amount of electrochemical storage to charge/discharge at time step t [kWh]
  - Dispatch time series of solar curtailment
    - c_t, amount of solar energy curtailed at time step t [kWh]
  - Dispatch time series of diesel dispatch
    - G_t, amount of electricity generated by diesel in each time step t [kWh]
    - D_t, binary variable to turn on diesel generator in each time step t [kWh]
- Dispatchable Load Decision Variables
  - Dispatch time series of CropBox HVAC
    - $Q^C{}_t$, electrical energy to run HVAC system at each time step t [kWh]
  - Dispatch time series of STP heat trace
    - Q^L_t, electrical energy to run STP heat trace at each time step t [kWh]
  - Dispatch time series of WR system treatment/heating
    - W_t, electrical energy to run WR system at each time step t [kWh]
- Objective
  - Minimize diesel generation costs

$$\min \sum_t C_G\, G_t + C_{OM}\, D_t \,|\, D_t - D_{t-1} \,|\, C_d \tag{A.1}$$

    - Where C_G is the cost of diesel generated electricity [$/kWh]
    - C_{OM} is the operations and maintenance cost of diesel [$/hr]
    - C_D is the cost of diesel dispatch start-up/cool-down [$/step]
- Defined Variables
  - Current amount of energy stored in battery storage

$$SE_{t+1} = SD\left[(c)E_{in,t} - (1/d)E_{out,t}\right] \tag{A.2}$$

    - Where c and d are the charging and discharging efficiencies respectively
  - Temperature, T, in CF, STP, and WR system container and hot water tank in time step t

$$T_{t+1} = T_t + (1/C)\left[\eta Q - UA(T_t - T_{amb})\right] \tag{A.3}$$

    - Where C is the thermal capacitance of water mass
    - UA is the heat loss coefficient
    - ηQ is the amount of heating/cooling delivered [kWh]
- Constraints
  - Overall electricity flows in the grid must be balanced in each time step

$$G_t + (S_t - c_t) + E_{out,t} = L_t + E_{in,t} \tag{A.4}$$

    - Where L_t is the total electrical load (including DSM) at time step t
  - Diesel generator must operate within its capacity (C) constraints:

$$G_t > 0.3G \tag{A.5}$$

$$G_t > G \tag{A.6}$$

  - Diesel generator must operate if minimum SOC set point of battery is reached:

$$D_t + SE_t / (E(SOC_{min})) < 1 \tag{A.7}$$

- Diesel generate must shut off when maximum SOC set point of battery is reached:

$$D_t + SE_t / \left(E\left(SOC_{max}\right) < 2 \right. \quad \text{(A.8)}$$

- Storage state of charge must lie within limits in each time step (for battery electrochemical storage, which is restricted by DOD:

$$DOD < SE_t < E \quad \text{(A.9)}$$

- Maximum heating/cooling and temperature constraints
- WR system tank capacity
- WR minimum treatment process time

References

[1] "Old crow solar project." https://www.acec.ca/awards/2019/a13.html (accessed Nov. 17, 2021).

[2] J. VanderMeer, M. Mueller-Stoffels, E. Whitney, An Alaska case study: energy storage technologies, J. Renew. Sustain. Energy 9 (6) (2017) 061708 Nov, doi:10.1063/1.4986580.

[3] E. Whitney, et al., MicroFEWs: A food–energy–water systems approach to renewable energy decisions in islanded microgrid communities in rural alaska, Environ. Eng. Sci. 36 (7) (2019) 843–849 Jul, doi:10.1089/ees.2019.0055.

[4] H.J. Jabir, J. Teh, D. Ishak, H. Abunima, Impacts of demand-side management on electrical power systems: a review, Energies 11 (5) (2018) 5ArtMay, doi:10.3390/en11051050.

[5] R.S. Kumar, L.P. Raghav, D.K. Raju, A.R. Singh, Intelligent demand side management for optimal energy scheduling of grid connected microgrids, Appl. Energy 285 (2021) 116435 Mar, doi:10.1016/j.apenergy.2021.116435.

[6] M.F. Zia, E. Elbouchikhi, M. Benbouzid, Microgrids energy management systems: a critical review on methods, solutions, and prospects, Appl. Energy 222 (2018) 1033–1055 Jul, doi:10.1016/j.apenergy.2018.04.103.

[7] A. Bhattacharjee, H. Samanta, A. Ghosh, T.K. Mallick, S. Sengupta, H. Saha, Optimized integration of hybrid renewable sources with long-life battery energy storage in microgrids for peak power shaving and demand side management under different tariff scenario, Energy Technol. 9 (9) (2021) 2100199, doi:10.1002/ente.202100199.

[8] N. Razmjooy, V.V. Estrela, R. Padilha, A.C.B. Monteiro, World cup optimization algorithm: application for optimal control of pitch angle in hybrid renewable PV/wind energy system, in: Metaheuristics and Optimization in Computer and Electrical Engineering, Springer International Publishing, Cham, 2021, pp. 25–47, doi:10.1007/978-3-030-56689-0_3. N. Razmjooy, M. Ashourian, and Z. Foroozandeh, Eds.,Lecture Notes in Electrical Engineering.

[9] G. Zhang, C. Xiao, N. Razmjooy, Optimal operational strategy of hybrid PV/wind renewable energy system using homer: a case study, Int. J. Ambient Energy 43 (1) (2022) 3953–3966 Dec, doi:10.1080/01430750.2020.1861087.

[10] P.S. Moura, A.T. de Almeida, Multi-objective optimization of a mixed renewable system with demand-side management, Renew. Sustain. Energy Rev. 14 (5) (2010) 1461–1468 Jun, doi:10.1016/j.rser.2010.01.004.

[11] A. Pina, C. Silva, P. Ferrão, The impact of demand side management strategies in the penetration of renewable electricity, Energy 41 (1) (2012) 128–137 May, doi:10.1016/j.energy.2011.06.013.

[12] G.R. Aghajani, H.A. Shayanfar, H. Shayeghi, Demand side management in a smart micro-grid in the presence of renewable generation and demand response, Energy 126 (2017) 622–637 May, doi:10.1016/j.energy.2017.03.051.

[13] N. Rezaei, M. Kalantar, Smart microgrid hierarchical frequency control ancillary service provision based on virtual inertia concept: An integrated demand response and droop controlled distributed generation framework, Energy Convers. Manag. 92 (2015) 287–301 Mar, doi:10.1016/j.enconman.2014.12.049.

[14] N. Ra, A. Ghosh, A. Bhattacharjee, IoT-based smart energy management for solar vanadium redox flow battery powered switchable building glazing satisfying the HVAC system of EV charging stations, Energy Convers. Manag. 281 (2023) 116851 Apr, doi:10.1016/j.enconman.2023.116851.

[15] V. García Tapia, Hybrid renewable energy system for controlled environment agriculture, Thesis, 2018.

[16] J.A. Houtman, Design and plan of a modified hydroponic shipping container for research part of the agriculture commons, art and design commons, and the bioresource and agricultural engineering commons recommended citation, 2016. [Online]. Available: https://docs.lib.purdue.edu/open_access_theses.

[17] R. Sparks, "Mapping and analyzing energy use and efficiency in a modified hydroponic shipping container," *Open Access Theses*, Aug. 2016, [Online]. Available: https://docs.lib.purdue.edu/open_access_theses/1011.

[18] D. Kirchem, M. Lynch, V. Bertsch, E. Casey, Modelling demand response with process models and energy systems models: Potential applications for wastewater treatment within the energy-water nexus, Appl. Energy 260 (2020) 114321 –114321Feb, doi:10.1016/j.apenergy.2019.114321.

[19] V.Z. Gjorgievski, N. Markovska, A. Abazi, N. Duić, The potential of power-to-heat demand response to improve the flexibility of the energy system: An empirical review, Renew. Sustain. Energy Rev. 138 (2021) 110489 Mar, doi:10.1016/j.rser.2020.110489.

[20] P. Kohlhepp, H. Harb, H. Wolisz, S. Waczowicz, D. Müller, V. Hagenmeyer, Large-scale grid integration of residential thermal energy storages as demand-side flexibility resource: A review of international field studies, Renew. Sustain. Energy Rev. 101 (2019) 527–547 Mar, doi:10.1016/j.rser.2018.09.045.

[21] D. Kanakadhurga, N. Prabaharan, Demand side management in microgrid: A critical review of key issues and recent trends, Renew. Sustain. Energy Rev. 156 (2022) 111915 Mar, doi:10.1016/j.rser.2021.111915.

[22] D. Groppi, A. Pfeifer, D.A. Garcia, G. Krajačić, N. Duić, A review on energy storage and demand side management solutions in smart energy islands, Renew. Sustain. Energy Rev. 135 (2021) 110183 Jan, doi:10.1016/j.rser.2020.110183.

[23] S. Iqbal, et al., A comprehensive review on residential demand side management strategies in smart grid environment, Sustainability 13 (13) (2021) Art. no. 13Jan, doi:10.3390/su13137170.

[24] D.J. Sambor, S.C.M. Bishop, A. Dotson, S. Aggarwal, M.Z. Jacobson, Optimizing demand response of a modular water reuse system in a remote Arctic microgrid, J. Clean. Prod. 346 (2022) 131110 Apr, doi:10.1016/j.jclepro.2022.131110.

[25] D. J. Sambor, M. Wilber, E. Whitney, M.Z. Jacobson, Development of a tool for optimizing solar and battery storage for container farming in a remote arctic microgrid, Energies 13 (19) (2020) 5143 –5143Oct, doi:10.3390/en13195143.

[26] H.P. Huntington, et al., Applying the food–energy–water nexus concept at the local scale, Nat. Sustain. 4 (8) (2021) 672–679 *2021 4*8May, doi:10.1038/S41893-021-00719-1.

[27] D. Mackay, Sustainable Energy without the Hot Air, University of Cambridge, 2008.

[28] "Freight Farms | Hydroponic shipping container farms," *Freight Farms*. https://www.freightfarms.com (accessed Nov. 17, 2021).

[29] K.A. Hickel, A. Dotson, T.K. Thomas, M. Heavener, J. Hébert, J.A. Warren, The search for an alternative to piped water and sewer systems in the Alaskan Arctic, Environ. Sci. Pollut. Res. 25 (33) (2018) 32873–32880 Nov, doi:10.1007/s11356-017-8815-x.

[30] C. Lucas, B. Johnson, E. Hodges Snyder, S. Aggarwal, A. Dotson, A tale of two communities: adopting and paying for an in-home non-potable water reuse system in Rural Alaska, ACS EST Water 1 (8) (2021) 1807–1815 Aug, doi:10.1021/acsestwater.1c00113.

[31] G. M. Masters, "Renewable and efficient electric power systems," p. 676. 2023.

[32] I. Dunning, J. Huchette, M. Lubin, JuMP: a modeling language for mathematical optimization, SIAM Rev. 59 (2) (2017) 295–320 Jan, doi:10.1137/15M1020575.

[33] Y. Sun, V. Venugopal, A.R. Brandt, Convolutional Neural Network for Short-term Solar Panel Output Prediction, in: Proceedings of the IEEE 7th World Conference on Photovoltaic Energy Conversion (WCPEC), 2018, pp. 2357–2361, doi:10.1109/PVSC.2018.8547400. *(A Joint Conference of 45th IEEE PVSC, 28th PVSEC 34th EU PVSEC)*Jun.